

# Diffractive photoproduction of opposite-charge pseudoscalar meson pairs at high energies

Antoni Szczurek<sup>1,3,4</sup> and Adam P. Szczepaniak<sup>1,2</sup>

<sup>1</sup> *Nuclear Theory Center, Indiana University,  
Bloomington, Indiana 47405, USA*

<sup>2</sup> *Physics Department, Indiana University,  
Bloomington, Indiana 47405, USA*

<sup>3</sup> *Institute of Nuclear Physics  
PL-31-342 Cracow, Poland*

<sup>4</sup> *University of Rzeszów  
PL-35-959 Rzeszów, Poland*

(Dated: November 19, 2018)

We calculate the cross section for diffractive photoproduction of opposite-charge pseudoscalar meson pairs  $M^+M^- = \pi^+\pi^-, K^+K^-, D^+D^-$  and  $B^+B^-$  in a broad range of center-of-mass energies relevant for GlueX/Hall D, FOCUS, COMPASS and HERA experiments. In the case of  $\pi^+\pi^-$  production we find that the interference of the  $\rho^0$  resonance and the two-pion continuum leads to a considerable deformation of the shape of  $\rho^0$  in agreement with the data from the ZEUS collaboration. We also discuss the spectral shape of the  $\rho^0$  as a function of the momentum transfer and the contribution of higher partial waves to the  $\pi^+\pi^-$  mass spectrum. We predict a sizeable energy-dependent forward-backward asymmetry in the Gottfried-Jackson frame. For the heavy meson production we find that the cross section for diffractive production increases much slower than the one for open charm or bottom production. We discuss lower and upper limits for the cross sections for diffractive production of  $D^+D^-$  and  $B^+B^-$  pairs, which we find can be as large as 10% of the open flavor production.

PACS numbers: 13.60.Le, 11.80.Et, 12.40.Nn

Keywords:

## I. INTRODUCTION

The mechanism of diffractive photoproduction of charged pion pairs has been proposed long ago [1, 2, 3, 4, 5, 6]. At that time there, however, no good data was available for constraining details of the model. In recent years a body of data from  $\pi N$  and  $KN$  scattering has been collected (see for instance [7]). In particular the ZEUS and H1 collaborations at HERA have measured diffractive production of the  $\rho^0$  meson. Most of the theoretical effort, however, concentrated on the description of the total cross section in different pQCD inspired approaches and not on the description of the two-pion continuum invariant mass distribution.

In real photoproduction the ZEUS collaboration observed a strong asymmetry in the two-pion invariant mass spectrum around the peak position [8] of the  $\rho^0$ . In electroproduction the asymmetry seems to decrease with increasing photon virtuality [9],  $Q^2$  and momentum transfer  $t' = |t - t_{min}|$  [10]. One would expect, whatever the non-resonant mechanism might be, that it will also be present at small  $Q^2$  and small  $t'$  and thus needed to isolate the  $\rho^0$  production cross section.

The GlueX (Hall D) project at the Jefferson Lab will study mesonic resonances focusing on gluonic excitations. The diffractive production of charged meson continuum may produce large backgrounds to the channels of interest. Recently exotic  $J^{PC} = 1^{-+}$  candidates have been reported by the E852 [11] and the Crystall Barrel [12] collaborations. Candidates for the exotic states are rather

broad [11, 12] and may indeed have a large component originating from production of the meson continuum production [13, 14].

Recently the FOCUS collaboration at Fermilab found a new state in the  $K^+K^-$  final state at 1.75 GeV [15] which may also require a good understanding of the  $K\bar{K}$ , continuum production.

In the present paper we study the  $\pi^+\pi^-$  and  $K^+K^-$  channels. In this case model ingredients are well constrained by the  $\pi N$  and  $KN$  data. The  $\pi^+\pi^-$  invariant mass distribution and possible  $\pi^+ - \pi^-$  polar angle asymmetries are presently being analyzed by the COMPASS collaboration [16]. We also compare the results of our calculation with the experimental data at higher energies from HERA and medium energy relevant for the future GlueX/Hall D experiment at TJNAF.

The inclusive production of heavy charmed mesons in electro- or pho-production off proton is routinely used to study the gluon distribution in the nucleon. The standard QCD approach is based on the production of heavy quark – heavy antiquark pairs at the parton level from photon-gluon fusion followed by a fragmentation to heavy flavored hadrons. The formalism which we present for diffractive production of pairs of light charged mesons should be also valid for the production of pairs of heavy mesons,  $D^+D^-$  or even  $B^+B^-$ . This may be interesting in the context of a deficit in the open  $b\bar{b}$  production in photon-proton [20] and photon-photon [21] collisions.

Recently the FOCUS collaboration has analyzed the azimuthal correlations between  $D\bar{D}$  mesons [22]. It was

pointed out very recently [23] that heavy meson correlations are very useful to study unintegrated gluon distributions in the nucleon. To the best of our knowledge, the contribution of the diffractive mechanism, discussed here, has not been estimated in this context. It is also interesting to investigate how large the diffractive production of  $B^+B^-$  pairs might be, compared to the standard pQCD mechanism of  $b\bar{b}$  production discussed above. In photoproduction, one would naively expect a relative enhancement of the ratio of diffractive  $B^+B^-$  (charge 1) to the standard  $b\bar{b}$  (charge 1/3) production as compared to the ratio of the  $D^+D^-$  (charge 1) to the  $c\bar{c}$  (charge 2/3) production by a factor of 4 in the cross section. A better understanding requires, however, more detailed insight into the dynamics of the process. In the present paper we shall present estimates of such contributions. In particular, we discuss several aspects of the opposite-charge pseudoscalar continuum in photoproduction.

We note that a similar model has been recently applied to describe  $\pi\pi$  and  $K\bar{K}$  photoproduction in Ref.[18].

## II. MODEL OF THE CONTINUUM

The dominant mechanisms of diffractive production of opposite-charge meson pairs are shown in Fig.1. The continuum production shown by the diagrams (a) and (b) in Fig.1 is often a background to direct resonance ( $\rho^0$ ,  $\phi$ ,  $f_2$ , etc.) production shown in diagram (c). We shall refer to (a)-(b) and (c) as the continuum and resonance contributions, respectively. The zigzag line represents the pomeron and subleading reggeon exchanges. The cross section for diffractive photoproduction of the opposite charge meson pairs, can be written as

$$d\sigma = (2\pi)^4 \delta^4(q + p - p_+ - p_- - p') \frac{d^3 p_+}{2\omega_+ (2\pi)^3} \frac{d^3 p_-}{2\omega_- (2\pi)^3} \frac{d^3 p'}{2\omega' (2\pi)^3} \times \frac{1}{flux} |\mathcal{M}^{\gamma p \rightarrow M^+ M^- p}|^2, \quad (1)$$

where for photoproduction,  $flux = 4\sqrt{(p \cdot q)^2 - m_p^2 q^2} = 2(s - m_p^2)$  and for a three-body reaction the amplitude  $[\mathcal{M}]$  carries dimension of  $\text{GeV}^{-1}$ . The unpolarized cross section is a function of the following variables, the square of the center of mass energy,  $s = (q + p)^2$ , the two-meson invariant mass,  $M_{MM}^2 = (k_+ + k_-)^2$ , the four-momentum transfer squared in the nucleon,  $t = (p - p')^2$  and the polar and azimuthal angles,  $\Omega = (\theta, \phi)$  specifying the direction of momentum of one of the two produced mesons in the two-meson recoil center of mass (RCM) system. The coordinates of the RCM system are usually chosen such that the  $y$  axis is perpendicular to the production plane determined by the photon and the recoil nucleon momenta, and  $z$  is chosen either in the direction of the photon momentum (in the RCM system), which

is then referred to as the Gottfried-Jackson (GJ), or  $z$  is anti-parallel to the recoiling nucleon direction, which defines the so called s-channel helicity (SCH). At high energy ( $s \gg M_{MM}^2, t$ ) the cross section takes a simple form

$$\frac{d\sigma(M_{MM}^2, t, \theta, \phi)}{dM_{MM}^2 dt d\Omega} = \frac{\beta}{16\pi^4} \frac{1}{s^2} |\mathcal{M}^{\gamma p \rightarrow M^+ M^- p}|^2, \quad (2)$$

where  $\beta = \sqrt{1 - \left(\frac{2m_M}{M_{MM}}\right)^2}$  is the magnitude of velocity of each meson in the center of mass of the  $M^+M^-$  system. The invariant amplitude for the  $2 \rightarrow 3$  continuum process can be written in the Regge factorized form corresponding to the diagrams (a) and (b) in Fig. 1,

$$\mathcal{M}_{\lambda_\gamma \lambda \rightarrow \lambda'}^{\gamma p \rightarrow M^+ M^- p}(s, t, s_+, t_+, s_-, t_-) = V_{\gamma M^+}(\lambda_\gamma) \frac{F_{os}(t_+)}{t_+ - m_M^2} \mathcal{M}_{\lambda \lambda'}^{M^- p}(s_-, t) + V_{\gamma M^-}(\lambda_\gamma) \frac{F_{os}(t_-)}{t_- - m_M^2} \mathcal{M}_{\lambda \lambda'}^{M^+ p}(s_+, t). \quad (3)$$

In the equation above  $s_+$  and  $s_-$  are the Mandelstam variables for the  $M^+p$  and  $M^-p$  elastic scattering and  $t_+$  and  $t_-$  are squares of momenta of the virtual mesons ( $t_\pm = (k_\pm - q)^2$ ). For pseudoscalar mesons, because  $q\epsilon_\pm(\lambda_\gamma = \pm 1) = 0$ , the corresponding vertex functions

read

$$V_{\gamma M^\pm}(\lambda_\gamma) = \pm e (2k_\pm^\mu) \epsilon_\mu(\lambda_\gamma). \quad (4)$$

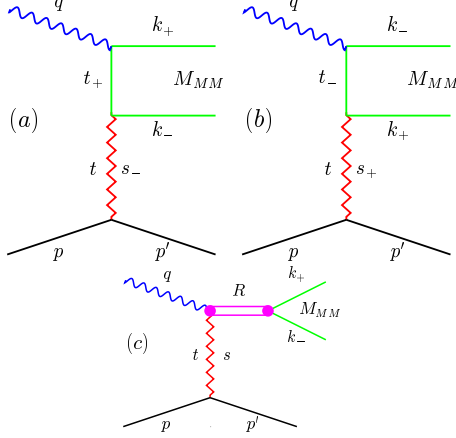


FIG. 1: Diffractive photoproduction of opposite-charge meson pairs. The wavy line corresponds to the photon, the zigzag line describes the pomeron and subleading reggeon exchanges, the lower lines are incoming and outgoing nucleons.

The matrix elements take a simple form in the Gottfried-Jackson frame,

$$\begin{aligned} \epsilon(\lambda_\gamma = \pm 1) \cdot k_+ &= \mp \frac{k}{\sqrt{2}} \sin(\theta_{GJ}) \exp(\pm i\phi_{GJ}) \\ \epsilon(\lambda_\gamma = \pm 1) \cdot k_- &= \pm \frac{k}{\sqrt{2}} \sin(\theta_{GJ}) \exp(\pm i\phi_{GJ}) \end{aligned} \quad (5)$$

The denominators in Eq.(3) can be calculated in terms of the canonical variables  $t$ ,  $M_{MM}$  and  $\cos\theta$  as

$$t_\pm - m_M^2 = -2qk_\pm = -\frac{1}{2}(M_{MM}^2 - t)(1 \mp \beta \cos\theta). \quad (6)$$

For small invariant masses  $M_{M^+M^-}$  of the two-meson state, (in the case of light meson production) sufficiently large overall  $s$  leads to large  $s_+$  and  $s_-$  in the relevant

subprocesses. At the high energies the invariant amplitudes for the  $2 \rightarrow 2$  quasi-elastic subprocesses can be written in the simple but rather accurate form,

$$\mathcal{M}_{\lambda\lambda'}^{M^\pm p}(s_\pm, t) = i s_\pm \sigma_{M^\pm p}^{tot}(s_\pm) \exp\left(\frac{B}{2}t\right) \delta_{\lambda\lambda'}. \quad (7)$$

The Kronecker  $\delta_{\lambda\lambda'}$  reflects explicit imposition of the target nucleon helicity conservation, known to hold at high energies. The total cross section for  $\pi p$  and  $Kp$  are well known [7] and at high energies one can use the Donnachie-Landshoff parametrizations [25]. For heavy mesons an educated guess will be necessary. In general, the heavier the mesons, the smaller the corresponding total cross section. The factor  $F_{os}(t_\pm)$  in Eq.(3) takes into account the extended nature of the exchanged particle. Since for the process considered there are two vertices with an off-shell pseudoscalar meson, it is natural to write the combined form factor in the factorized form:

$$F_{os}(t_\pm) = F_{em}^{hos}(Q^2, t_\pm, m_M) \cdot F_{corr}(t_\pm), \quad (8)$$

where the first factor is the half-off-shell electromagnetic form factor from the upper vertex and the second one is a form factor representing the middle vertices in diagrams (a) and (b) in Fig.1. The exact form of the form factors is not known. In principle, a good quality data would help to find the proper functional form.

Energy conservation imposes natural limits on energies in different two-body subsystems

$$\begin{aligned} W_+ &\equiv \sqrt{s_+} < W - m_M, \\ W_- &\equiv \sqrt{s_-} < W - m_M, \\ M_{MM} &< W - m_p. \end{aligned} \quad (9)$$

The amplitude given in Eq.(3) is not yet complete since it does not satisfy electromagnetic current conservation. This current is given by,

$$J^\mu = 2e \left[ k_+^\mu \frac{F_{os}(t_+)}{t_+ - m_M^2} \mathcal{M}_{\lambda\lambda'}^{M^- p}(s_-, t) - k_-^\mu \frac{F_{os}(t_-)}{t_- - m_M^2} \mathcal{M}_{\lambda\lambda'}^{M^+ p}(s_+, t) \right] \quad (10)$$

so that the amplitude in Eq.(3) can be written as,

$$\mathcal{M}_{\lambda_\gamma \lambda \rightarrow \lambda'}^{\gamma p \rightarrow M^+ M^- p} = \epsilon_\mu(\lambda_\gamma) J^\mu(s, t, s_+, t_+, s_-, t_-) \quad (11)$$

Current conservation implies  $q_\mu J^\mu = 0$  while from Eq.(10) we find

$$\begin{aligned} q_\mu J^\mu &= -4e \left[ F_{os}(t_+) \mathcal{M}_{\lambda\lambda'}^{M^- p}(s_-, t) \right. \\ &\quad \left. - F_{os}(t_-) \mathcal{M}_{\lambda\lambda'}^{M^+ p}(s_+, t) \right]. \end{aligned} \quad (12)$$

The origin of current non-conservation is two-fold. It comes from the non-point-like nature of the exchanged

particles which introduces the form factors,  $F_{os} \neq 1$  and from the difference in meson-nucleon scattering for the two charged mesons. The latter implies that electromagnetic charge flows differently in  $M^+ p \rightarrow M^+ p$  and  $M^- p \rightarrow M^- p$  subprocesses and since photon couples to all charge currents there has to be a correction which reflects this difference.

Having identified the two sources which contribute to the current we can unambiguously find the required corrections. We want to separate the corrections to the current which arise from interactions in the upper (meson)

and lower (baryon) vertices and therefore we define,

$$F_{\pm} \equiv \frac{1}{2} [F_{os}(t_+) \pm F_{os}(t_-)] \quad (13)$$

and

$$M_{\pm} \equiv \frac{1}{2} [\mathcal{M}_{\lambda\lambda'}^{M^-p}(s_-, t) \pm \mathcal{M}_{\lambda\lambda'}^{M^+p}(s_+, t)] \quad (14)$$

The current can be written as

$$J^{\mu} = J_C^{\mu} + J_N^{\mu} + J_M^{\mu} \quad (15)$$

where

$$J_C^{\mu} = 2e \left[ \frac{k_+^{\mu}}{t_+ - m_M^2} - \frac{k_-^{\mu}}{t_- - m_M^2} \right] (F_+ M_+ + F_- M_-) \quad (16)$$

is a conserved current,

$$J_N^{\mu} = 2e \left[ \frac{k_+^{\mu}}{t_+ - m_M^2} + \frac{k_-^{\mu}}{t_- - m_M^2} \right] F_+ M_- \quad (17)$$

is non-conserved due to a difference between  $M^+N$  and  $M^-N$  cross-sections, and

$$J_M^{\mu} = 2e \left[ \frac{k_+^{\mu}}{t_+ - m_M^2} + \frac{k_-^{\mu}}{t_- - m_M^2} \right] F_- M_+ \quad (18)$$

is non-conserved due the extended structure of the exchanged meson. Now the additional contribution to the current required by current conservation will depend on meson variables for  $J_M^{\mu}$  and nucleon variables for  $J_N^{\mu}$ , respectively,

$$J_N^{\mu} \rightarrow J_N^{\mu} + \delta J_N^{\mu} \quad (19)$$

with

$$\delta J_N^{\mu} = 2e \frac{(p + p')^{\mu}}{q(p + p')} F_+ M_- \quad (20)$$

and

$$J_M^{\mu} \rightarrow J_M^{\mu} + \delta J_M^{\mu} \quad (21)$$

with

$$\delta J_N^{\mu} = 2e \frac{(k_+ + k_-)^{\mu}}{q(k_+ + k_-)} F_- M_+ = -4e \frac{(k_+ + k_-)^{\mu}}{t - M_{MM}^2} F_- M_+ \quad (22)$$

The the unphysical pole at  $t = M_{MM}^2$ , Eq.(22) should be eliminated by a zero in the  $F_-$  form factor vanishes at  $t = M_{MM}^2$ .

In Fig.2 we show the effect of these corrections on the angular distribution for  $\pi^+\pi^-$  production calculated in the GJ frame. The correction is generally very small, except for the tips of the angular distributions.

In this example we have integrated over the invariant mass range  $M_{\pi\pi} = 0.45-0.95$  GeV and over the kinematically accessible range of the momentum transfer  $t$ . It

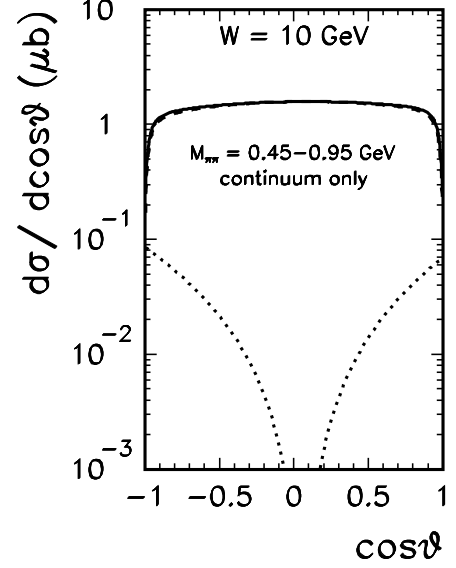


FIG. 2: Angular distribution of  $\pi^+$  in the Gottfried-Jackson frame. The dashed line is the contribution without corrections restoring current conservation. The dotted line represent the cross section associated with the corrections itself and the solid line corresponds to the full, current conserving amplitude. In this calculation we used the monopole off-shell form factor with  $M_{os} = 1$  GeV (see Eq.(32)).

is easy to check that the correction is negligible for the invariant mass distribution.

In this paper we shall concentrate on the distributions in  $M_{MM}$  and  $\cos\theta$ . Often one is interested in distributions in the s-channel helicity frame and not in the Gottfried-Jackson frame. From the definition of the two frames it follows that the spherical angles in the GJ frame can be expressed by those in the SCH frame  $\mathcal{M}_{\lambda_\gamma}^{\gamma p \rightarrow M^+ M^- p}(t, M_{MM}, \theta_{GJ}, \phi_{GJ})$ , with  $\theta_{GJ} = \theta_{GJ}(\theta_{SCH}, \phi_{SCH})$  and  $\phi_{GJ} = \phi_{GJ}(\theta_{SCH}, \phi_{SCH})$  through a rotation around the  $y$  axis by an angle  $\theta_{rot}$  [26] which in the high energy limit is given by,

$$\cos\theta_{rot} = \frac{M_{MM}^2 + t}{M_{MM}^2 - t} \quad (23)$$

In Fig.3 we compare angular distributions for the continuum in the Gottfried-Jackson (left panel) and in the s-channel helicity (right panel) frames. The shapes in both frames are rather different. The effect of the rotation was neglected in the early calculations.

In order for the Regge parametrization of the two-body amplitudes to be reliable, for  $\pi^+\pi^-$  production the energies  $W_+, W_-$  have to be at least larger than 2 GeV. This can be fulfilled for center of mass energy  $W > 4$  GeV, i.e.  $E_\gamma > 8$  GeV. The future GlueX experiment at TJNAF

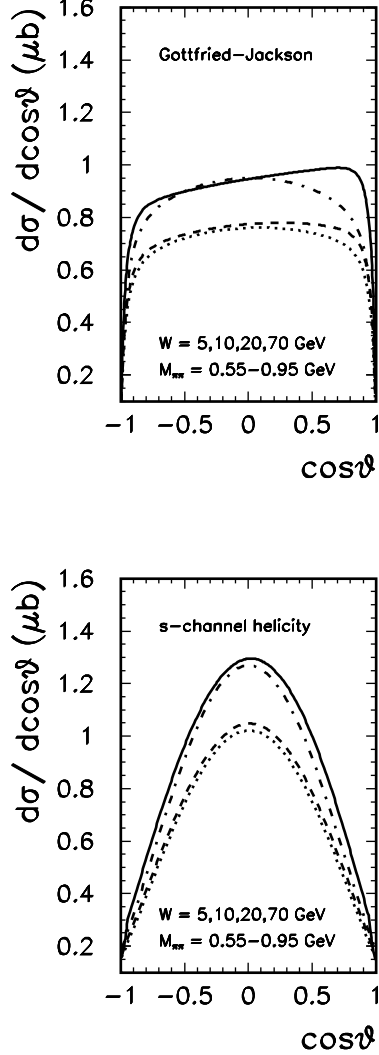


FIG. 3: Angular distributions of  $\pi^+$  from continuum amplitude in the Gottfried-Jackson (left panel) and in the s-channel helicity (right panel) frames for four different energies:  $W = 5$  GeV (solid),  $W = 10$  GeV (dashed),  $W = 20$  GeV (dotted) and  $W = 70$  GeV (dash-dotted). In this calculation we used the monopole off-shell form factor with  $M_{os} = 1$  GeV (see Eq.(32)).

is therefore at the border of application of the present model.

### III. RESULTS

The cross section for a three-body reaction depends on five independent kinematical variables. For the reactions considered it is customary to use  $M_{MM}$ ,  $t$ ,  $\theta$  and  $\phi$  and calculate  $d\sigma(M_{MM}, t, \Omega)/dM_{MM}dt d\Omega$ . The invariant mass distribution is then obtained by integrating over the remaining variables

$$\frac{d\sigma}{dM_{MM}} = \int_{t_{min}(M_{MM})}^{t_{max}(M_{MM})} dt d\Omega \frac{d\sigma(M_{MM}, t, \Omega)}{dM_{MM}dt d\Omega}, \quad (24)$$

where  $t_{min}$  and  $t_{max}$  are calculated from the three-body kinematics (see for instance [30]).

#### A. Light meson pairs

Below  $M_{\pi\pi} = 1$  GeV the  $\rho^0$  meson dominates the two-pion invariant mass spectrum. The amplitude for the resonance is taken in the relativistic Breit-Wigner form. In our simple approach the normalization constant at  $t = 0$  is fixed based on the vector meson dominance model. We write the resonant three-body amplitude as,

$$\mathcal{M}_{\lambda_\gamma \lambda \rightarrow \lambda'}^{\gamma \rightarrow \rho^0 \rightarrow \pi^+ \pi^-}(s, t, M_{\pi\pi}, \theta, \phi) = C_{conv} \frac{e}{\gamma_\rho} \mathcal{M}_{\lambda \lambda'}^{\rho^0 p}(s, t) f_{BW}(M_{\pi\pi}) Y_{1, \lambda_\gamma}(\theta, \phi). \quad (25)$$

Here we have introduced the amplitude for quasi-elastic scattering of  $\rho^0$  meson off the proton

$$\mathcal{M}_{\lambda \lambda'}^{\rho^0 p}(s, t) = i s \sigma_{\rho^0 p}^{tot}(s) \exp\left(\frac{B_{\rho p} t}{2}\right) \delta_{\lambda \lambda'}. \quad (26)$$

As for the continuum model the Kronecker  $\delta_{\lambda \lambda'}$  reflects high-energy helicity conservation in the proton vertex. The factor  $C_{conv}$  is adjusted to reproduce the correct normalization of the amplitude.

Different normalization of the reaction amplitudes are used in the literature. Throughout the present paper we use a popular in high-energy diffraction (see e.g. [24]) normalization, such that the angular distribution for the two-body reaction is

$$\frac{d\sigma}{d\Omega_{CM}} = \frac{1}{64\pi^2 s} \left( \frac{p_f}{p_i} \right) |\overline{\mathcal{M}}_{fi}|^2 \quad (27)$$

and the optical theorem at high energy reads

$$\text{Im}\mathcal{M}(s, t=0) = s\sigma^{tot}(s). \quad (28)$$

This fixes the  $C_{conv}$  factor in Eq.(25).

The factor  $f_{BW}$  is the standard relativistic Breit-Wigner propagator,

$$f_{BW}(M_{\pi\pi}) = \frac{\sqrt{M_0\Gamma(M_{\pi\pi})/\pi}}{M_0^2 - M_{\pi\pi}^2 - iM_0\Gamma(M_{\pi\pi})}, \quad (29)$$

where  $\Gamma(M_{\pi\pi}) = \Gamma_0 \left( \frac{M_{\pi\pi}^2 - 4m_\pi^2}{M_0^2 - 4m_\pi^2} \right)^{3/2}$ . and it is normalized according to  $\int |f_{BW}(M_{\pi\pi})|^2 dM_{\pi\pi}^2 = 1$  if  $\Gamma(M_{\pi\pi})$  is replaced by the energy independent width,  $\Gamma_0$ . We take  $M_0 = 768$  MeV and  $\Gamma_0 = 151$  MeV and

$$\sigma_{\rho^0 p}^{tot}(s) = \frac{1}{2} \left( \sigma_{\pi^+ p}^{tot}(s) + \sigma_{\pi^- p}^{tot}(s) \right). \quad (30)$$

As for the continuum model the total cross sections for  $\pi^+ p$  and  $\pi^- p$  are taken from the Donnachie-Landshoff parametrization [25]. In the present approach we assume the same slope parameter for the resonance and continuum contributions,  $B_{\rho p} = B_{\pi p} \equiv B$ . Except for the off-shell dependence determined by the form factors  $F_{os}$  our model is essentially parameter free. We used different parametrizations the form factor: the exponential form,

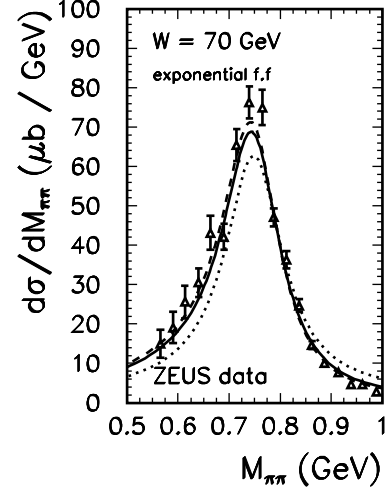
$$F_{os}(t_\pm) = \exp\left(\frac{t_\pm - m_M^2}{2\Lambda_{os}^2}\right) \quad (31)$$

and the monopole form

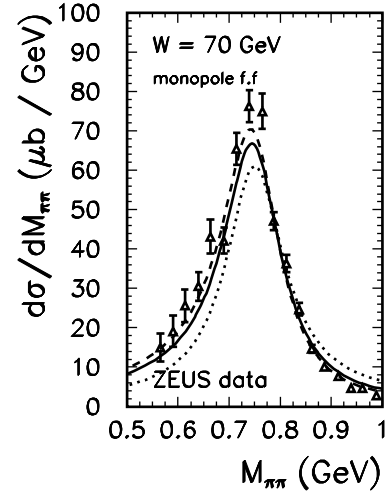
$$F_{os}(t_\pm) = \frac{M_{os}^2 - m_M^2}{M_{os}^2 - t_\pm}. \quad (32)$$

The form factor is normalized to unity at the on-shell point  $t = m_M^2$ . The exponential form is useful as the universal parameter  $\Lambda_{os}$  for different meson exchanges can be used. In the monopole parametrization  $M_{os} > m_M$ , *i.e.* different cut-off parameters for different exchanges have to be used. On the other hand the monopole form seems to be preferred, because at small virtualities vector dominance applies and in addition it produces a correct pQCD dependence at large virtualities.

The off-shell form factor is the least know element of our model. In Figs.4, 5 we present spectral shape (resonance + continuum) for the two choices of from factors without and with rotation from SCH to GJ frame. Somewhat better agreement is obtained without performing the extra rotation of arguments.



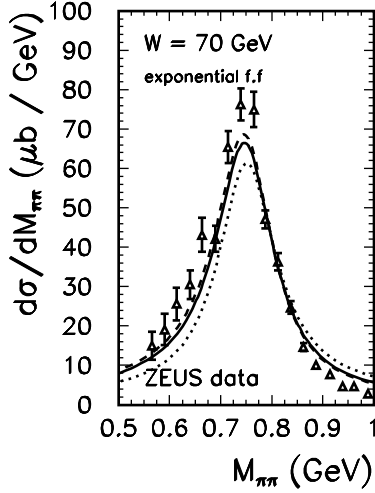
(a)



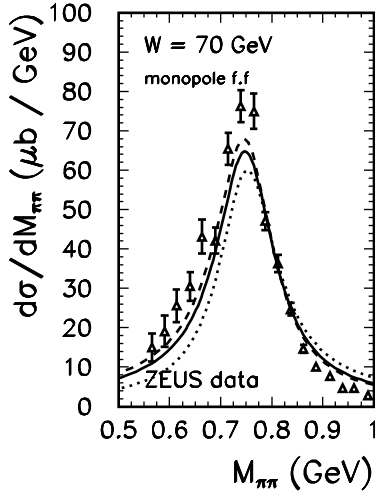
(b)

FIG. 4: The spectrum of invariant mass  $M_{\pi\pi}$  for  $W = 70$  GeV for exponential and monopole off-shell form factor without rotation of continuum arguments. The experimental results of the ZEUS collaboration are from [8]. In this calculation  $B = 8 \text{ GeV}^{-2}$ .

The spectral shape depends on the value of the form factor parameter ( $\Lambda_{os} = 0.5, 1.0, 2.0$  GeV for the exponential form factor, and  $M_{os} = 0.5, 1.0, 2.0$  GeV for the monopole form factor). For pion production very similar results are obtained with exponential and monopole form factors for  $\Lambda_{os} \approx M_{os}$ . Therefore, having in view a possible universality of the exponential off-shell form factor parameter  $\Lambda_{os}$ , we shall use the exponential form factor in the following. The experimental data from the ZEUS collaboration at DESY [8] are superimposed on the theoretical lines. In the absence of other mechanisms the value of the off-shell form factor could be obtained from



(a)



(b)

FIG. 5: Same as in Fig. 4 but with rotation of continuum arguments.

the fit to the experimental data. The coherent sum of the resonance and continuum (solid line) differs considerably from the standard resonance shape which is shown in Fig. 6. The resonance contribution alone (dashed line) gives a poor description of the data. In particular, the position of the maximum is at higher  $m_{\pi\pi}$  than observed experimentally. These features have been often ignored in the literature and only integrated cross section were used to compare with theoretical calculations.

In order to have a better insight into the origins of the line-shape modifications in Fig. 7 we show separately the resonance and the continuum contributions in somewhat broader range of two-pion invariant mass. This figure clearly demonstrates that it is mainly the interference

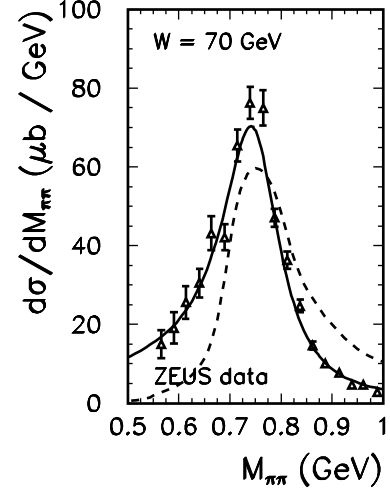


FIG. 6: The spectrum of invariant mass  $M_{\pi\pi}$  for  $W = 70$  GeV. The experimental results of the ZEUS collaboration are from [8]. In this calculation  $B = 8 \text{ GeV}^{-2}$ . The standard resonance contribution is shown as a reference (dashed line).

effect which deforms the spectral shape of the  $\rho$  meson.

In our approach the background is described by a physical process which has a strong two-pion invariant mass dependence. Often in experimental analyses [8, 9, 10] (see also [27]), this background is parametrized with a weak  $\pi\pi$  mass dependence. We do not expect that our model could describe the experimental spectra above  $M_{\pi\pi} > 1 \text{ GeV}$ , since there will be important contributions from higher mass two-pion resonances *e.g.*  $f_2(1270)$ ,  $\rho_3(1690)$ ,  $\rho(1700)$ . The situation there may be therefore rather complicated and we leave the corresponding analysis for future investigations.

In order to further understand the large interference effect of the continuum contribution with the  $P$ -wave resonance we performed a decomposition of the continuum amplitude into the partial wave series in the GJ frame,

$$\begin{aligned} \mathcal{M}_{\lambda_\gamma, \lambda \rightarrow \lambda'}^{\gamma p \rightarrow M^+ M^- p}(t, M_{\pi\pi}, \theta, \phi) = \\ = \sum_{l, m} a_{lm}^{\lambda_\gamma, \lambda, \lambda'}(t, M_{\pi\pi}) Y_{lm}(\theta, \phi). \end{aligned} \quad (33)$$

The expansion coefficients can be calculated as

$$\begin{aligned} a_{lm}^{\lambda_\gamma, \lambda, \lambda'}(t, M_{\pi\pi}) = \\ = \int Y_{lm}^*(\theta, \phi) \cdot \mathcal{M}_{\lambda_\gamma, \lambda \rightarrow \lambda'}^{\gamma p \rightarrow M^+ M^- p}(t, M_{\pi\pi}, \theta, \phi) d\Omega. \end{aligned} \quad (34)$$

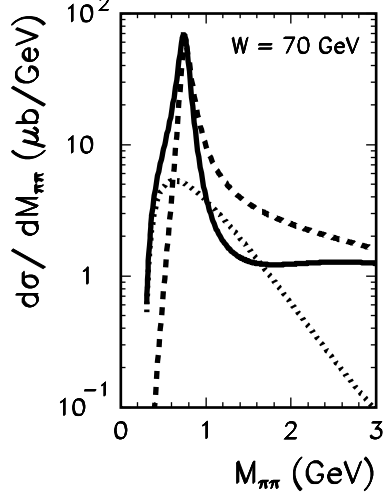


FIG. 7: The decomposition of the spectrum of the  $\pi^+\pi^-$  invariant mass  $M_{\pi\pi}$  for  $W = 70$  GeV. We show separately the resonance (dashed line) and continuum (dotted line) cross sections. The solid line corresponds to a coherent sum of both processes. In this calculation  $B = 8 \text{ GeV}^{-2}$ .

In our model the expansion coefficients depend only on  $\lambda_\gamma, l, m$ , i.e.

$$a_{lm}^{\lambda_\gamma, \lambda, \lambda'}(t, M_{\pi\pi}) \equiv a_{lm}^{\lambda_\gamma}(t, M_{\pi\pi}). \quad (35)$$

We find that in the case of the pseudoscalar production the continuum contributes dominantly to the  $P$ -wave, *i.e.*  $|a_{1m}| \gg |a_{00}|, |a_{2m}|$ , etc. and  $|a_{1-1}^{+1}| < |a_{10}^{+1}| < |a_{1+1}^{+1}|$ , and  $|a_{1-1}^{-1}| > |a_{10}^{-1}| > |a_{1+1}^{-1}|$ . This explains the large interference between the continuum and resonance production. We also find a relatively large contribution of the  $F$ -wave. The individual contributions of  $l = 1$  and  $l = 3$  partial wave are shown in Fig.8.

Presence of the  $F$ -wave is interesting in the context of forward-backward asymmetry and the moment analysis (see e.g.[19]). These are usually discussed in terms of the  $S$ - and  $P$ - wave interferences. Our analysis shows that in principle one needs to include  $S, P, D$  and  $F$  waves into such an analysis even for relatively low invariant masses.

Let us try to understand this hierarchy of the partial wave amplitudes. The angular distribution originates from

$$\begin{aligned} \mathcal{M}_{\lambda_\gamma}^{\gamma p \rightarrow M^+ M^- p}(t, M_{MM}, \theta, \phi) \\ \propto q_{MM} i \mathcal{F}(t) \exp(\pm i \phi) \sin \theta \mathcal{A}(\theta, \phi), \end{aligned} \quad (36)$$

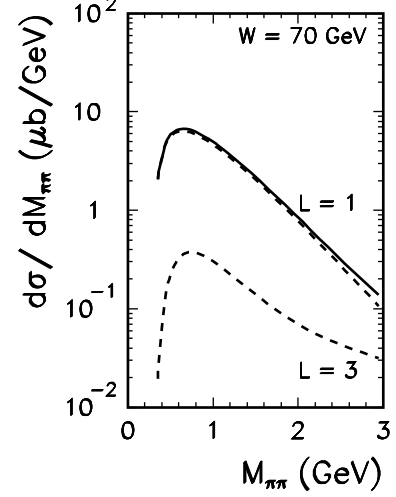


FIG. 8: The contributions of individual partial waves to the spectrum of invariant mass  $M_{\pi\pi}$  for  $W = 70$  GeV (excluding resonance production). In this calculation  $B = 8 \text{ GeV}^{-2}$ .

where we have defined a slowly changing function of  $\theta$  and  $\phi$ ,

$$\begin{aligned} \mathcal{A}(\theta, \phi) = & \frac{\sigma_{M-p}(s_-(\theta, \phi)) F_{os}(t_+(\theta))}{1 - \beta \cos \theta} \\ & + \frac{\sigma_{M+p}(s_+(\theta, \phi)) F_{os}(t_-(\theta))}{1 + \beta \cos \theta}. \end{aligned} \quad (37)$$

It then becomes obvious that it is the function  $\mathcal{A}(\theta, \phi)$  which is responsible for generation of partial waves different than  $l = 1$ . It is easy to show that if the numerators were identical the  $S$ -wave amplitude would vanish. The smooth energy dependence of the cross sections introduces a small  $S$ -wave contribution. This small effect is slightly dependent on the incident energy.

The large interference effect is specific to the photoproduction of  $P$ -wave resonances and the  $P$ -wave dominated pseudoscalar meson continuum.

In Fig.9 we discuss the evolution of the spectral shape (asymmetry) as a function of the momentum transfer,  $|t|$ . While at low  $|t|$  the spectral asymmetry is reversed compared to the standard resonant shape at large  $|t|$  one observes a restoration of the standard asymmetry expected for the  $P$ -wave resonance. Such an effect was observed experimentally in [10] and to the best of our knowledge the dynamics of this effect has not been given before.

So far we have neglected the final state  $\pi\pi$  interaction. This can be restored by modifying the continuum partial-wave amplitudes,

$$\tilde{a}_{lm}^{\lambda_\gamma, \lambda, \lambda'} = a_{lm}^{\lambda_\gamma, \lambda, \lambda'} \cos \delta_l^{\pi\pi} \exp(i \delta_l^{\pi\pi}). \quad (38)$$

Here  $\delta_l^{\pi\pi}$  is the  $M_{\pi\pi}$ -dependent phase shift for  $\pi\pi$  scattering in the  $l$ 'th partial wave. If only resonant final state



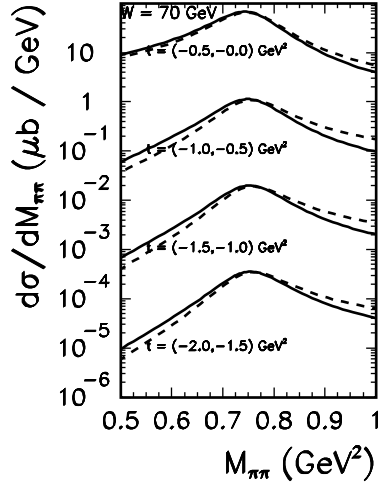


FIG. 9: The spectrum of invariant mass  $M_{\pi\pi}$  for  $W = 70$  GeV for different bins in  $t$ . The solid lines correspond to the results without and the dashed line to the results with the rotation of arguments of the continuum contribution. In this calculation  $B = 8 \text{ GeV}^{-2}$  and exponential off-shell form factor with  $\Lambda = 1 \text{ GeV}$  has been used.

interaction effects are included the modified partial amplitude of the continuum becomes,

$$\tilde{a}_{lm}^{\lambda_\gamma, \lambda, \lambda'} = a_{lm}^{\lambda_\gamma, \lambda, \lambda'} \left( \frac{M_{\pi\pi}^2 - M_0^2}{M_{\pi\pi}^2 - M_0^2 + iM_0\Gamma} \right). \quad (39)$$

Such a modified amplitude vanishes at  $M_{\pi\pi} = M_0$ . For  $l = 1$  the final amplitude can be written as a sum of three terms: the direct  $\rho^0$  production, free meson pair production and the resonance production via re-scattering. The last two are contained in Eq.(39) (or Eq.(38)). We checked that re-scattering from the continuum back to the resonance is negligible.

The  $K^+K^-$  production is more sensitive to the choice of the off-shell form factor. The spectrum of two-kaon invariant mass is shown in Fig.10 for exponential form factor and  $\Lambda_{os} = 0.5, 1.0, 2.0 \text{ GeV}$ .

Recent experimental data from the FOCUS collaboration are shown for comparison [15]. Our model of diffractive production of kaonic pairs gives a good description of the main trend of the data. A direct comparison with the FOCUS data is, however, not possible, because the experimental acceptance is known only in very limited range of the phase space. The absolutely normalized experimental invariant mass distribution would help to better limit the only unknown parameter  $\Lambda_{os}$  (or  $M_{os}$ ) of the off-shell form factor. The situation may be, however, not so simple in light of recent experimental data for  $\gamma\gamma$  collisions [17]. In principle, similarly as for the  $\pi^+\pi^-$  invariant mass the interference of the  $K^+K^-$  continuum and the  $\phi$  resonance takes place. However, because the  $\phi$  has a

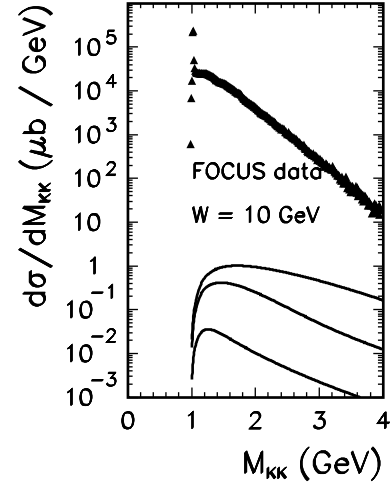


FIG. 10: The spectrum of invariant mass  $M_{K\bar{K}}$ . The experimental results of the FOCUS collaboration (without acceptance corrections) are from [31]. The experimental data is not normalized. In this calculations  $B = 6 \text{ GeV}^{-2}$  and exponential off-shell form factor with  $\Lambda = 0.5, 1.0, 2.0 \text{ GeV}$  has been used.

much smaller decay width than the  $\rho^0$  and is situated very close to the  $K^+K^-$  threshold (where the continuum contribution is small), its importance for  $M_{KK} > 1.1 \text{ GeV}$  is negligible.

The angular distributions depend on the invariant mass. Thus one studies angular distributions in bins of invariant masses. The angular distribution is calculated from the 4-dimensional differential cross section as,

$$\frac{d\sigma}{d\cos\theta} = \int_{M_{min}}^{M_{max}} dM_{MM} \int_{t_{min}}^{t_{max}} dt \int d\phi \frac{d\sigma(M_{MM}, t, \Omega)}{dM_{MM} dt d\Omega}. \quad (40)$$

In Fig.11 we present angular distribution for the ZEUS kinematics [8]. The angular distribution is almost proportional to  $(\sin\theta)^2$ . The continuum contribution only slightly modifies the  $(\sin\theta)^2$  resonance distribution. The results with or without rotation between the frames are almost indistinguishable.

In Fig.12 we present predictions for angular distributions for the GlueX experiment at TJNAF. The shape of the distributions depends on the interval of the two-pion invariant mass. The effect of the rotation of the arguments of the continuum is stronger for smaller invariant masses. We predict a sizable asymmetry with,  $\pi^+$  being preferentially emitted in the forward (photon) direction.

The function  $\mathcal{A}(\theta, \phi)$  in Eq.(36) is responsible not only for generating higher partial waves but also for the forward-backward asymmetry. In order to measure the

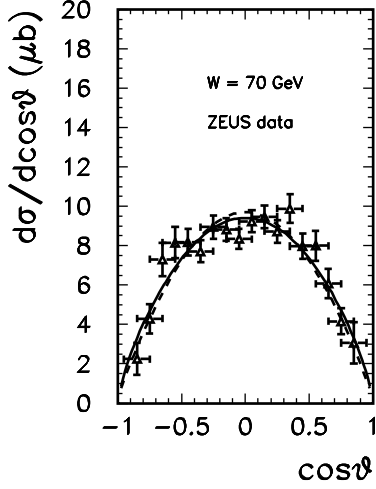


FIG. 11: The angular distribution of charge pions in the SCH frame for  $W = 70$  GeV and  $M_{\pi\pi}$  in the measured range. The experimental results of the ZEUS collaboration are from [8]. In this calculation  $B = 8 \text{ GeV}^{-2}$  and exponential off-shell form factor with  $\Lambda = 1 \text{ GeV}$  have been used. The solid line corresponds to the calculation without rotation of arguments of the continuum, whereas the dashed line corresponds to the calculation with the rotation.

asymmetry we define the following quantity,

$$A_{FB}^{\pi^\pm}(\theta) \equiv \frac{\frac{d\sigma^{\pi^\pm}}{dz}(\theta) - \frac{d\sigma^{\pi^\pm}}{dz}(\pi - \theta)}{\frac{d\sigma^{\pi^\pm}}{dz}(\theta) + \frac{d\sigma^{\pi^\pm}}{dz}(\pi - \theta)}. \quad (41)$$

By construction

$$\frac{d\sigma}{d\theta}(\theta_{\pi^+}) = \frac{d\sigma}{d\theta}(\pi - \theta_{\pi^-}), \quad (42)$$

which means that the asymmetry must fulfil the symmetry relations

$$\begin{aligned} A_{FB}^{\pi^+}(\theta) &= -A_{FB}^{\pi^-}(\theta), \\ A_{FB}^{\pi^\pm}(\theta) &= -A_{FB}^{\pi^\pm}(\pi - \theta). \end{aligned} \quad (43)$$

The asymmetry for  $\pi^+$  is shown in Fig.13 for four different energies and for one bin in  $M_{\pi\pi}$ ,  $0.55 \text{ GeV} < M_{\pi\pi} < 0.95 \text{ GeV}$  and  $|t| < 1 \text{ GeV}^2$ . We present separately the asymmetry of the continuum contribution alone (panel a) and the asymmetry of the sum of the resonance and continuum contributions (panel b). A sizable asymmetry can be seen in the GJ frame (solid lines). In general, the larger incident energy, the smaller the asymmetry. The inclusion of the resonance contribution lowers the asymmetry around  $z = 0$ .

For the GlueX experiment at TJNAF we predict the asymmetry to be about 10% at the very forward and very

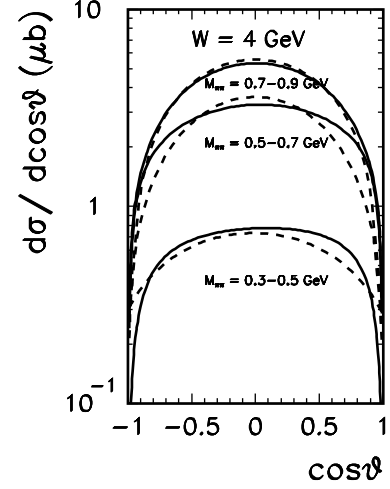


FIG. 12: The angular distribution of  $\pi^+$  in the SCH frame for the GlueX energy  $W = 4 \text{ GeV}$ . In this calculation  $B = 6 \text{ GeV}^{-2}$  and exponential off-shell form factor with  $\Lambda = 1 \text{ GeV}$  have been used. The solid line corresponds to the case of no extra rotation while dashed line corresponds to the result with the extra rotation.

backward directions. Even at  $W = 70 \text{ GeV}$  the asymmetry is of the order of 1%. In our model the asymmetry is caused by the different interaction of  $\pi^+p$  and  $\pi^-p$  (analogously for  $K^+p$  and  $K^-p$ ). This is caused by a different strength of sub-leading reggeons. The asymmetry disappears at large energy where the dynamics of elastic scattering is governed exclusively by the pomeron exchange. The asymmetry discussed above is an important test of the diffractive mechanism. When transformed to the SCH frame the asymmetry becomes rather negligible (dashed lines).

In Refs.[32, 33] the observation of forward-backward asymmetry of charged pions was proposed in order to pin down the odderon exchange. These analyses were based on the assumption that only resonant mechanisms plays a role. The mechanism considered here was not taken into account. Our diffractive mechanism may mimic the pomeron-odderon interference effects discussed in Refs.[32, 33]. A careful search for the odderon exchange must therefore necessarily include the two-pion continuum discussed in the present paper.

We expect that the diffractive production of  $K^+K^-$  is the dominant mechanism well above the  $\phi$  resonance. In Fig.14 we present angular distributions of  $K^+$  in the GJ recoil center of mass system for a typical FOCUS energy,  $W = 10 \text{ GeV}$  for different bins of  $M_{KK}$  specified in the figure.

As for the pion production we obtain asymmetric distributions with  $K^+$  being preferentially emitted in the forward hemisphere. The shape of the angular distribution changes with  $M_{KK}$ . The shape is very important

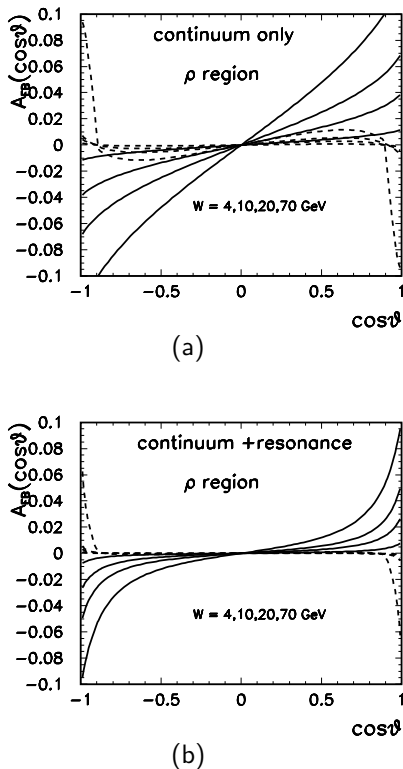


FIG. 13: Forward-backward asymmetry for  $\pi^+$  for the continuum (panel a) and for the resonance+continuum (panel b) as the function of  $\cos\theta$  for four different energies:  $W = 4, 10, 20, 70$  GeV. The solid line corresponds to the continuum in the GJ, while the dashed line to the continuum in the SCH frame. The kinematical cuts are specified in the text.

when studying resonances. For example, the FOCUS collaboration found difficulties in spin assignment of the  $X(1750)$  [31]. This may partially be due to the interference of the resonance and the continuum. In general, the larger the invariant mass, the more the cross section peaks at forward/backward directions. This is related to the increase in the number of active partial waves with the increasing subsystem energy.

In Fig.15 we present  $A_{FB}$  for  $K^+$  for four different incident energies,  $1.9 \text{ GeV} < M_{KK} < 2.1 \text{ GeV}$  and  $|t| < 1 \text{ GeV}^2$ . We observe much larger asymmetries than for the  $\pi^+\pi^-$  case. This is partially due to larger asymmetries in  $K^+p$  and  $K^-p$  scattering than for the  $\pi^+p$  and  $\pi^-p$  scattering.

In principle the  $K^+K^-$  asymmetry should be seen in the data of the FOCUS collaboration. The possible higher mass resonance contributions are expected to lower the asymmetry. A careful search for the asymmetry as a function of the two-kaon invariant mass would be very interesting in searches for new states.

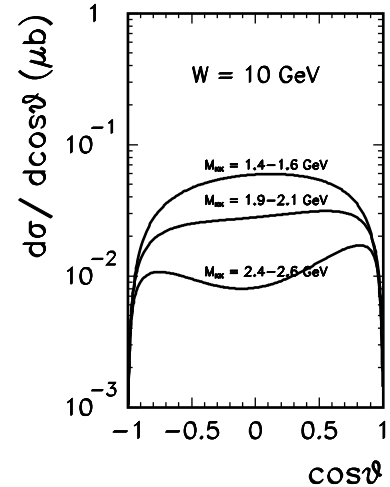


FIG. 14: The angular distribution of  $K^+$  in the GJ frame for a typical FOCUS energy  $W = 10$  GeV. In this calculation  $B = 6 \text{ GeV}^{-2}$ .

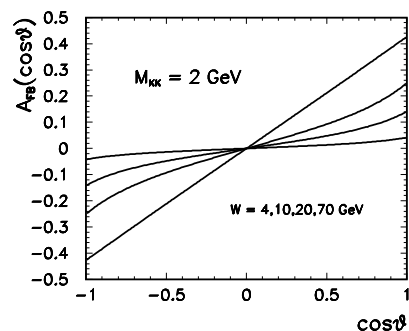


FIG. 15: Forward-backward asymmetry for  $K^+$  production in the GJ frame as the function of  $\cos\theta$  for four different energies:  $W = 4, 10, 20, 70$  GeV. The kinematical cuts are specified in the text.

## B. Heavy meson pairs

In Fig.16 we show invariant mass distributions of diffractively produced pairs of  $D^+D^-$  for the average energy of the FOCUS experiment [22].

The averaging is not so important as the diffractive contribution is only slowly dependent on the incident energy. We show results for different values of the scale parameter in the exponential off-shell form factor. The absolute normalization strongly depends on the value of the form factor mass parameter. This is due to the fact that the intermediate meson  $D$  in Fig.1 is far from its mass shell. Our distributions peak at  $M_{DD} = 4.5\text{--}5 \text{ GeV}$ . In principle, the FOCUS collaboration could an-

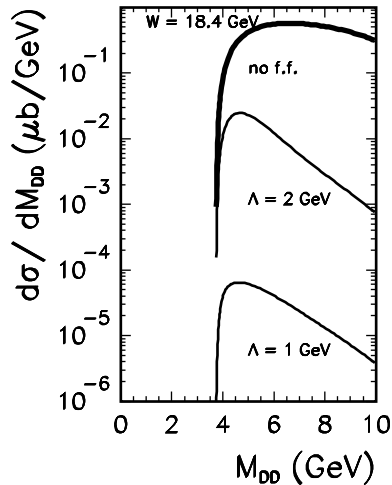


FIG. 16: The spectrum of invariant mass  $M_{DD}$ . The theoretical results were obtained with  $B = 6 \text{ GeV}^{-2}$  and exponential off-shell form factor with parameters specified in the figure.

alyze their data and try to construct the invariant mass distribution. The expected statistics will be of course rather low, of the order of 10-50 events.

The invariant mass distribution for the  $B^+B^-$  pair production is shown in Fig.17 for a typical HERA energy  $W = 100 \text{ GeV}$ . Here there is a dramatic effect on the value of the form factor parameter. The distribution reaches its maximum at rather high  $M_{BB}$ . The smallness of the cross sections precludes, however, studies of differential cross section.

In Figs.18, 19 we show the energy dependence of the integrated cross section for both  $DD$  and  $BB$  pair production (thick solid line). For comparison we show the standard collinear-factorization results for open charm and open bottom production [34] as well as the experimental cross sections. As can be seen from the figure the diffractive cross section is much smaller than its counterpart for the standard photon-gluon fusion followed by fragmentation.

In addition, the rise of the cross section with energy is slower than for the photon-gluon fusion. Only close to the kinematical threshold the diffractive component may constitute a sizable fraction of the open heavy-flavor component. Since in this case application of the meson-exchange approach is less reliable than for the light pairs, an experimental measurement would be very interesting and helpful to discriminate between models. While for the  $D^+D^-$  pairs this may be feasible, it will be hard to expect such an analysis for the  $B^+B^-$  pairs, at least in a few year perspective. We predict the fraction of diffractive-to-nondiffractive events to be somewhat larger for bottom than for charm mesons.

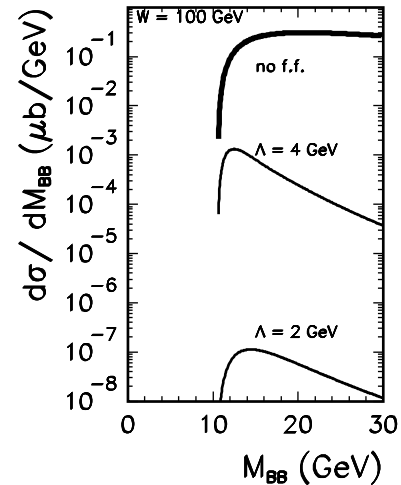


FIG. 17: The spectrum of invariant mass  $M_{BB}$ . The theoretical results were obtained with  $B = 6 \text{ GeV}^{-2}$  and exponential off-shell form factor with parameters specified in the figure.

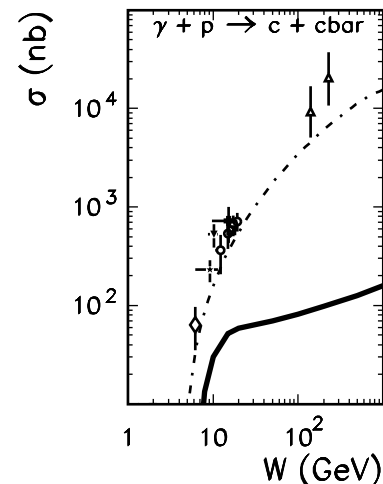


FIG. 18: The energy dependence of the integrated cross section for the diffractive photoproduction of  $D^+D^-$  (thick solid line) with our estimate of the upper limit ( $\Lambda_{os} = 2 \text{ GeV}$ ). For comparison we show the cross section for open charm and bottom production (dash-dotted line) and corresponding experimental data. The details concerning the open heavy-flavour production can be found in Ref.[34].

#### IV. CONCLUSIONS

We have presented a model of diffractive photoproduction of opposite-charge pseudoscalar mesons. The model should be valid at sufficiently high energies, down to energies relevant at the future experiments in Hall D at

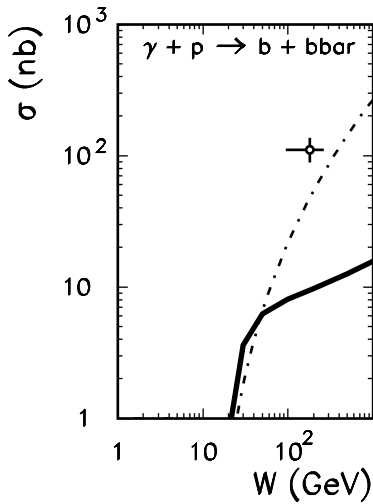


FIG. 19: Same as in Fig. 18 for  $B^+B^-$  production, ( $\Lambda_{os} = 4$  GeV).

Jefferson Lab. The understanding of the two-meson continua is absolutely crucial when looking for new (exotic) mesonic states in the two-meson channels. Our model results seem to be consistent with the current experimental data.

The interference of the two-pion continuum and the resonant  $\rho^0$  contribution leads to a significant deformation of the resonance peak, which is consistent with the experimental data from the ZEUS collaboration at HERA [8]. The effect of the continuum-resonance interference is often completely neglected. We explain a change of the spectral shape of the  $\rho^0$  bump with momentum transfer.

The diffractive mechanism of the  $K^+K^-$  production leads to a broad bump in invariant mass distribution, above the  $\phi$  meson position with the maximum at

$M_{KK} \approx 1.4$  GeV. Experimentally, except for the  $X(1750)$  mentioned earlier no clear resonances in the  $K^+K^-$  channel have been seen in [15] *e.g.* even though states like  $a_2$ ,  $f_2$ ,  $\rho_3$  are expected. A careful phase-shift analysis will be required to separate them. Our model amplitude provides a reasonably well controlled background for such studies.

We have found a forward-backward asymmetry in  $\pi^+$  and  $\pi^-$  (similarly  $K^+$  and  $K^-$ ) recoil center of mass angular distributions. The new effect is due to different interaction of different-charge mesons with the proton. The effect disappears at large incident energies, where the pomeron exchange is dominant. This asymmetry may be very important in the context of recently proposed searches for odderon exchange via forward-backward charge asymmetry in the region of  $M_{\pi\pi} \sim 1 - 2$  GeV.

The cross sections for diffractive production of heavy meson pairs were neither calculated nor measured in the past. In the present paper we have presented an estimates of the corresponding cross sections. The cross sections obtained in our analysis are, however, very small. Even a measurement of integrated cross section for diffractive  $D^+D^-$  pair photoproduction would be very useful for testing the mechanism of diffractive production. Such data would allow one to pin down off-shell effects for the intermediate (exchanged) heavy meson.

### Acknowledgments

We thank Ryan Mitchell for providing us the experimental two-kaon invariant mass distribution of the FOCUS collaboration. We are also indebted to Leonard Leśniak and Geoffrey Fox for several discussions. This work was partially supported by the US Department of Energy grant DE-FG0287ER40365 (APS), and the Nuclear Theory Center at Indiana University.

- 
- [1] S.D. Drell, Phys. Rev. Lett. **5**, 278 (1960).
  - [2] P. Söding, Phys. Lett. **19**, 702 (1965).
  - [3] A.S. Krass, Phys. Rev. **159**, 1496 (1967).
  - [4] G. Kramer and J.L. Uretsky, Phys. Rev. **181**, 181 (1969).
  - [5] J. Pumplin, Phys. Rev. **D2**, 1859 (1970).
  - [6] G. Kramer and H.R. Quinn, Nucl. Phys. **B27**, 77 (1971).
  - [7] Review of Particle Physics, Particle Data Group, Eur. Phys. J. **C15**, 1 (2000).
  - [8] M. Derrick et al. (ZEUS collaboration), Z. Phys. **C69**, 39 (1995).
  - [9] J. Breitweg et al. (ZEUS collaboration), Eur. Phys. J. **C6**, 603 (1999).
  - [10] J. Breitweg et al. (ZEUS collaboration), Eur. Phys. J. **C14**, 213 (2000).
  - [11] D.R. Thompson et al. (E852 collaboration), Phys. Rev. Lett. **79**, 1630 (1997).
  - [12] A. Abele et al. (Crystal Barrel collaboration), Phys. Lett. **B423**, 175 (1998).
  - [13] A. R. Dzierba *et al.*, Phys. Rev. **D 67**, 094015 (2003).
  - [14] A. P. Szczepaniak, M. Swat, A. R. Dzierba and S. Teige, Phys. Rev. Lett. **91**, 092002 (2003).
  - [15] J.M. Link et al. (FOCUS collaboration), Phys. Lett. **B545**, 50 (2002).
  - [16] A. Sandacz (COMPASS collaboration), private communication.
  - [17] K. Abe et al. (BELLE collaboration), Eur. Phys. J. **C32**, 323 (2003).
  - [18] Ch-R. Ji, R. Kamiński, L. Leśniak, A. Szczepaniak and R. Williams, Phys. Rev. **C58**, 1205 (1998).
  - [19] L. Bibrzycki, L. Leśniak and A.P. Szczepaniak, Eur. Phys. J. **C34**, 335 (2004).
  - [20] S. Chekanov et al. (ZEUS collaboration),

- hep-ex/0405069.
- [21] A. Csilling (OPAL collaboration), in *PHOTON2004, Ambleside, UK, August 26-31, 2000*, hep-ex/0011022; M. Acciari et al. (L3 collaboration), Phys. Lett. **B503**, 10 (2001); F. Kapusta (DELPHI collaboration), in *MESON2004, Cracow, Poland, June 4-8, 2004*.
  - [22] J.M. Link et al. (FOCUS collaboration), Phys. Lett. **B566**, 51 (2003).
  - [23] M. Łuszczak and A. Szczurek, Phys. Lett. **B594**, 291 (2004).
  - [24] V. Barone and E. Predazzi, *it High-Energy Particle Diffraction*, (Springer, Berlin 2002).
  - [25] A. Donnachie and P.V. Landshoff, Phys. Lett. **B296**, 227 (1992).
  - [26] K. Schilling, P. Seyboth and G. E. Wolf, Nucl. Phys. B **15**, 397 (1970) [Erratum-ibid. B **18**, 332 (1970)].
  - [27] M.G. Ryskin and Yu.M. Shabelski, Phys. Atom. Nucl. **61**, 81 (1998).
  - [28] D.C. Fries et al., Nucl. Phys. B **143**, 408 (1978).
  - [29] D.P. Barber et al., Z. Phys. **D12**, 1 (1982).
  - [30] E. Byckling and K. Kajantie, *Particle Kinematics*, (John Wiley and Sons, London 1973).
  - [31] R.E. Mitchell, *Phd thesis, the University of Tennessee, Knoxville, December 2003*.
  - [32] Ph. Hagler, B. Pire, L. Szymanowski and O.V. Teryaev, Eur. Phys. J. **C26**, 261 (2002).
  - [33] I.F. Ginzburg, I.P. Ivanov and N.N. Nikolaev, Eur. Phys. J. **C30**, 2 (2003).
  - [34] A. Szczurek, Eur. Phys. J. **C26**, 183 (2003).